JOURNAL OF VIROLOGY, Jan. 2005, p. 1071–1083 Vol. 79, No. 2
0022-538X/05/$08.00+0 doi:10.1128/JVI.79.2.1071–1083.2005

Impairment of Nuclear Pores in Bovine Herpesvirus 1-Infected MDBK Cells

Peter Wild,[1]* Monika Engels,[2] Claudia Senn,[2] Kurt Tobler,[2] Urs Ziegler,[3] Elisabeth M. Schraner,[1] Eva Loepfe,[2] Mathias Ackermann,[2] Martin Mueller,[4] and Paul Walther[5]

Electron Microscopy, Institute of Veterinary Anatomy,[1] Institute of Virology,[2] and Institute of Anatomy,[3] University of Zürich, and Center for Electron Microscopy, Institute of Applied Physics, Swiss Federal Institute of Technology,[4] Zürich, Switzerland, and Electron Microscopic Unit, University of Ulm, Ulm, Germany[5]

Received 5 July 2004/Accepted 17 August 2004

Herpesvirus capsids originating in the nucleus overcome the nucleocytoplasmic barrier by budding at the inner nuclear membrane. The fate of the resulting virions is still under debate. The fact that capsids approach Golgi membranes from the cytoplasmic side led to the theory of fusion between the viral envelope and the outer nuclear membrane, resulting in the release of capsids into the cytoplasm. We recently discovered a continuum from the perinuclear space to the Golgi complex implying (i) intracisternal viral transportation from the perinuclear space directly into Golgi cisternae and (ii) the existence of an alternative pathway of capsids from the nucleus to the cytoplasm. Here, we analyzed the nuclear surface by high-resolution microscopy. Confocal microscopy of MDBK cells infected with recombinant bovine herpesvirus 1 expressing green fluorescent protein fused to VP26 (a minor capsid protein) revealed distortions of the nuclear surface in the course of viral multiplication. High-resolution scanning and transmission electron microscopy proved the distortions to be related to enlargement of nuclear pores through which nuclear content including capsids protrudes into the cytoplasm, suggesting that capsids use impaired nuclear pores as gateways to gain access to the cytoplasmic matrix. Close examination of Golgi membranes, rough endoplasmic reticulum, and outer nuclear membrane yielded capsid-membrane interaction of high identity to the budding process at the inner nuclear membrane. These observations signify the ability of capsids to induce budding at any cell membrane, provided the fusion machinery is present and/or budding is not suppressed by viral proteins.

Herpesviruses comprise the capsid containing the viral genome, the viral envelope consisting of a lipid bilayer with embedded glycoproteins, and tegument proteins filling the space between capsid and envelope. DNA double strands formed during replication are packed into capsids built of proteins imported from the cytoplasm (32). Capsids are transported to the nuclear periphery. Their pathway through the nucleocytoplasmic barrier and the acquisition of tegument and envelope are yet not fully understood (18). Capsids bud through the inner nuclear membrane into the perinuclear space, concomitantly acquiring an envelope (15) and tegument proteins (43). It is assumed that the envelope derived from budding at the inner nuclear membrane fuses with the outer nuclear membrane, releasing both tegument and capsid into the cytoplasmic matrix (4, 6, 7, 12, 14–16, 20, 42, 46). Capsids are then transported to the trans-Golgi network, where they are wrapped by Golgi membranes leading to an enveloped virion within a transport vacuole. Alternatively, it is speculated that virions escape from the perinuclear space via vesicle formation at the outer nuclear membrane (5, 7, 11, 16, 31, 37). These vesicles then pass the Golgi complex for final maturation of virions. Contradictory to both the fusion and vesicle formation theory is the fact that fully enveloped virions were found in the perinuclear space and rough endoplasmic reticulum (RER) (13, 16, 31, 33, 34, 42), implying that virions are transported within the RER system. Connectivity between RER and the Golgi complex (28, 40, 43) makes it very likely that virions are transported from the perinuclear space via the RER into the Golgi complex for packaging into transport vacuoles (43). If this theory of intracisternal transport is correct, an alternative pathway for capsids entering the cytoplasmic matrix must exist as has been postulated for herpes simplex virus type 1 (3) and simian agent 8 (2).

The amount of membranes required for budding is enormous, considering that more than 1,000 capsids may be produced within a single nucleus. If the fusion theory were correct, membrane constituents would have to recycle from the outer to the inner nuclear membrane. If the vesicle formation theory were correct, membranes would have to be supplied for both the viral envelope deriving from the inner membrane and the vesicle membrane originating at the outer nuclear membrane. If the intracisternal transportation theory were correct, membrane constituents lost by budding at the inner nuclear membrane would have to be replaced. In any case, dramatic membrane translocation would be expected at one or both nuclear membranes while release of capsids via budding is going on.

Cells infected with bovine herpesvirus 1 (BoHV-1) disintegrate in the course of virus multiplication. This most likely involves fast disintegrating processes. The rapidity of cell disintegration suggests dramatic distortions within the nucleus and/or at the nuclear envelope. Such fast events can only be

* Corresponding author. Mailing address: Peter Wild Electron Microscopy Institute of Veterinary Anatomy, Winterthurerstrasse 266a, CH-8057 Zürich, Switzerland. Phone: 41 1 635 87 84. Fax: 41 1 635 89 11. E-mail: pewild@vetanat.unizh.ch.

recognized by electron microscopy, provided the temporal resolution of the preparation methods applied is sufficient. In addition, structures must be kept in place during the follow-up preparation or during observation in the electron microscope to visualize disintegrating processes such as the breakdown of membranes. High temporal resolution sufficient to study processes that take place in the millisecond range is achieved by rapid freezing of cellular or subcellular material down to liquid nitrogen temperatures. Loss of material can be prevented by examination of samples in the frozen hydrated state either by cryo-transmission electron microscopy (cryo-TEM), cryoscanning electron microscopy (cryo-SEM), or transmission electron microscopy (TEM) of specimens dehydrated at low temperatures (LTEM) (41).

To identify nuclear distortions, we investigated living cells infected with green fluorescent protein (GFP)-labeled BoHV-1 by confocal laser scanning microscopy to get an idea about the time course of virus multiplication in individual cells and the rapidity of their disintegration and correlated the findings by conventional TEM (CTEM). We then reconstructed nuclei from images obtained by confocal microscopy after fixation and DAPI (4′,6′-diamidino-2-phenylindole) staining, and employed cryo-field emission SEM (cryo-FESEM) of rapidly frozen, freeze-fractured, and platinum-shadowed cells (39). Finally, the nuclear surface and behavior of cell membranes were investigated at high resolution by LTEM. Here, we show that nuclear pores become impaired in the course of BoHV-1 multiplication while nuclear membranes and the plasma membrane seem to remain morphologically intact until the onset of disintegration. Distortion of nuclear pores seems to function as a gateway for capsids to pass the nucleocytoplasmic barrier rather than to play an essential role in cell disintegration.

MATERIALS AND METHODS

Viruses and cells. Madin Darby bovine kidney (MDBK) cells were grown in Dulbecco's modified Eagle's medium (Gibco, Bethesda, Md.) supplemented with 10% fetal calf serum (Gibco) at 37°C and 5% CO_2. Wild-type BoHV-1 (strain Jura) (27) and recombinant BoHV-1 were propagated in MDBK cells as described elsewhere (10).

Generation of recombinant BoHV-1. BoHV-1-specific sequences flanking the open reading frame of UL35 (encoding VP26) were amplified by PCR in two separate amplification reactions with primer pair UL35+ (5′-CGCATG CAT GGC GTC GTC GAA CCG CGA GTG-3′) and UL34− (5′-CCA TCA CGG CGG AGC AGA ACA ACG CC-3′) or UL35− (5′-ACGCCA TGC ATG CGC CTG CCG GGA TCG ACC-3′) and UL36+ (5′-GCG CGG CAC GGG CAT AAG CGT CCT GG-3′). Both amplification products were cloned and combined in pGEM-3Zf(+) such that a single NsiI site was introduced at the initiation codon of UL35. By site-directed mutagenesis, a single XhoI site was inserted between the putative poly(A) signal of UL35 and UL36, which was subsequently used for the insertion of a tetracycline-resistant gene under the control of a bacterial promoter amplified from pBR322 using the primer pair TET+ (5′-CTTCTC GAG TTC TCA TGT TTG ACA GCT TAT-3′) and TET− (5′-GGA CTC GAG AAA AAT CAC TCA GGG TCA ATG-3′). The resulting plasmid was designated p129. The GFP gene was amplified by PCR from pEGFP-N3 (Clontech) using the primer pair GFP+ (5′-CACCAT GCA TAG CAA GGG CGA GGA GCT GTT C-3′) and GFP− (5′-GCC CTG CAG CTT GTA CAG CTC GTC CAT GCC-3′). The ends of the PCR product were digested with NsiI and PstI and ligated into p129, resulting in p131. The linear fragment of p131 comprising the fusion protein gene GFP-UL35 and the gene for tetracycline resistance under the control of a bacterial promoter, flanked by BoHV-1-specific sequences, was amplified by PCR primer pair UL36+ and UL34−. The plasmid DNA, which served as template for the PCR amplification, was subsequently digested with DpnI, and the DpnI-resistant amplification product was used for insertion into electrocompetent and arabinose-induced *Escherichia coli* strain DH10B harboring f115.003, the wild-type BoHV-1 bacterial artificial chromosome (BAC) (36), and pKD46, which were selected on LB agar plates containing tetracycline. Recombinant BoHV-1 BAC DNA was amplified in *E. coli* and purified.

Recombinant BoHV-1 was reconstituted by the introduction of recombinant BoHV-1 BAC DNA into MDBK cells as previously described (36). The genomic integrity of recombinant BoHV-1 expressing the GFP-VP26 fusion protein (rBoHV-1–GFP–VP26) was analyzed by restriction enzyme digestion and PCR analysis. The functionality of the fusion protein gene was proven by fluorescence microscopy.

Infection of cells. MDBK cells were grown for 2 days either in petri dishes with a glass slide bottom (Mattek, Ashland, Mass.) for confocal time-lapse microscopy on coverslips for confocal analysis of nuclear alterations, in petriPERM dishes (Sartorius, Göttingen, Germany) for cryo-FESEM, or on 30-μm-thick sapphire disks with a diameter of 3 mm (Bruegger, Minusio, Switzerland) for LTEM, correlative confocal microscopy, and CTEM. Dishes, coverslips, and sapphire disks were covered with 8- to 10-nm-thick carbon obtained by evaporation under high-vacuum conditions to enhance cell growth. Then cells were infected with BoHV-1 at a multiplicity of infection (MOI) of 1, 5, and 10 or with rBoHV-1–GFP–VP26 (MOI, 0.5), and kept at 4°C for 1 h to admit adsorption prior to incubation at 37°C for up to 42 h.

Confocal microscopy. Time-lapse microscopy was performed with a confocal laser scanning microscope (model SP2; Leica, Mannheim, Germany) equipped with an environmental chamber at 37°C and 5% CO_2. For nuclear analyses, cells were fixed with 4% paraformaldehyde and stained with DAPI in phosphate-buffered saline (1 μg/ml). Samples were embedded in fluorescence mounting medium (DakoCytomation, Glostrup, Denmark) and analyzed by confocal laser scanning microscopy. Images were deconvolved with a blind deconvolution algorithm using the Huygens Essential program suite (SVI, Hilversum, The Netherlands).

Freezing of cells. Disks, 2 mm in diameter, were cut out of the petriPERM dishes (Sartorius) with an ophthalmologic punch and transferred into hexadecane (35) prior to being placed into an aluminum chamber with a central cavity (height, 50 μm; diameter, 2 mm). The sandwich was then placed in the holder of the high-pressure freezer (EM HPM; Wohlwend Engineering, Sennwald, Switzerland) and immediately frozen. Cells grown on sapphire disks were frozen in a similar manner in an HPM010 freezer (BAL-TEC, Inc., Balzers, Liechtenstein) as described in detail previously (43). The frozen samples were stored in liquid nitrogen until use.

Cryo-FESEM. The sandwich with the cells on the petriPERM disks within the aluminum planchets were clamped in a special holder (38) and cryofractured in a freeze-etching machine (BAF 300; BAL-TEC, Balzers, Liechtenstein) by removing one aluminum platelet with the microtome (temperature, −110°C, vacuum about 2×10^6 to 7×10^6 mPa). After 2 min of etching (sublimation of some water at the fracture face), the sample was double-layer coated (39) by electron beam evaporation with 3 nm of platinum-carbon from an angle of 45° and about 8 nm of carbon perpendicularly. The frozen sample was then mounted on a cryoholder (Gatan, Pleasanton, Calif.) and transferred into the microscope (S-5200 FESEM; Hitachi, Tokyo, Japan). The whole center of the punched-out petriPERM disk (about 1 mm^2) was analyzed at a temperature of −130°C and an acceleration voltage of 10 kV. Micrographs were recorded digitally with the back-scattered electron signal (39).

LTEM. Frozen cells grown on sapphire disks were transferred into a freeze-substitution unit (FS 7500; Boeckeler Instruments, Tucson, Ariz.) precooled to −88°C for substitution with acetone and subsequent fixation with 0.25% glutaraldehyde and 0.5% osmium tetroxide at temperatures between −30°C and 0°C as described previously in detail (44) and embedded in Epon. Sections (50 to 60 nm thick) were analyzed in a TEM (CM12; Philips, Eindhoven, The Netherlands) equipped with a slow scan charge-coupled device camera (Gatan) at an acceleration voltage of 100 kV.

CTEM. Cells grown on sapphire disks were fixed in 2.5% glutaraldehyde in 0.1 mM Na–K phosphate (pH 7.4) at 4°C for 1 h, postfixed in 1% osmium tetroxide in 0.1 mM Na–K phosphate (pH 7.4) at 4°C for 1 h, and dehydrated in acetone, followed by embedding, polymerization, and sectioning. To identify fluorescence signals, rBoHV-1–GFP–VP26-infected cells grown on carbon-coated sapphire disks were fixed with paraformaldehyde and examined by light microscopy with the areas of interest photographed and marked on the carbon film. After postfixation with glutaraldehyde and osmium tetroxide and processing for TEM, sections were cut from the area of interest, and cells were identified at low magnification.

RESULTS

Virus multiplication and fate of cells. Cells infected with rBoHV-1–GFP–VP26 (MOI, 0.5) emitted faint to strong sig-

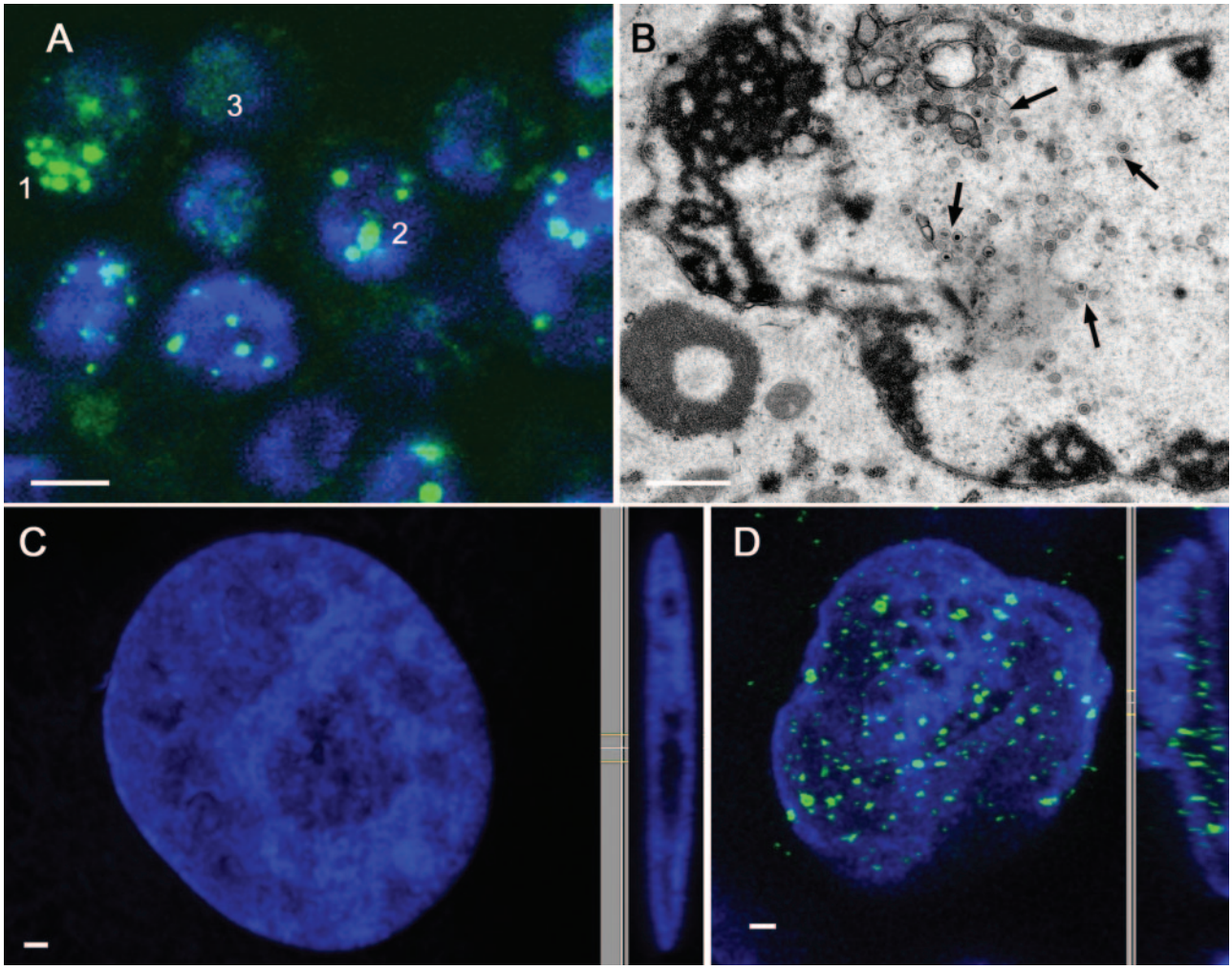

FIG. 1. MDBK cells infected with recombinant BoHV-1 (MOI, 0.5) expressing the GFP-VP26 fusion protein. (A) Cells after 42 h of incubation, fixation, and DAPI staining. The intense signals in cells 1 and 2 correspond to the accumulation of capsids and/or virions embedded in protein within the nucleus and cytoplasm (1) or only within the nucleus (2). Nuclear fragments and membranes, despite lost integrity, were recognized by CTEM. (B) Micrograph obtained by CTEM from cell 3 with only a faint fluorescence signal. The nucleus bears single capsids (arrows), capsids in small clusters, and membranous inclusions. Chromatin is condensed at the periphery, indicating apoptosis, and the nuclear membrane is intact. (C) Deconvolution of the nucleus after fixation and DAPI staining of a noninfected cell. The disk-like nucleus has diameters of 18.5, 15, and 2.5 μm and a calculated surface of 133 μm^2. (D) Deconvolution of a nucleus after fixation and DAPI staining of an infected cell incubated for 42 h. The disk-like irregularly shaped nucleus with the short diameter of about 3.5 μm contains irregularly distributed chromatin and accumulation of capsids. The surface is calculated to be approximately 160 μm^2. Bars, 10 μm (A); 1 μm (B to D).

nals 28 h postinfection as detected by confocal microscopy (data not shown). To monitor the fate of infected cells, we chose cells emitting light signals at 28 h of infection for time-lapse microscopy at intervals of 6 min up to 42 h. Emission of signals enhanced drastically in a given cell first as diffusely distributed spots and later as bright patches (Fig. 1A). Correlative CTEM revealed that the finely dispersed signals were derived from capsids (Fig. 1B) or virions and that the bright patchy signals were derived from structures referred to as inclusion bodies, comprising accumulated GFP-VP26 (data not shown). Some cells disappeared rapidly in the course of incubation, whereas others remained intact for hours despite of accumulation of vast fluorescent material. Although the integrity of membranous compartments was lost to various extents in cells shown to be intact or healthy by light microscopy, intact plasma membranes and fragmented nuclei or nuclei with peripheral chromatin condensation, capsids, and membranous inclusions could be seen (Fig. 1B). Deconvolution of DAPI-stained nuclei of uninfected cells revealed disk-like structures with long diameters of more than 18 μm and short diameters of only 2.5 μm (Fig. 1C). The chromatin of infected cells turned out to be very irregular, with protrusions and depressions (Fig. 1D). The longest diameter of nuclei was 14 to 15 μm, and the shortest was up to 3.5 μm. To get an idea of size differences, we estimated the nuclear surface area from DAPI-stained DNA on the basis of the means of the long and short diameters, assuming that the nuclear surface was smooth. In doing so, the nuclear surface area was approximately 130 μm^2 in cells chosen at random at the beginning of incubation and about 160 μm^2 in cells chosen at random that had been

incubated for 42 h (that is, about 14 h of signal generation). The true surface of irregularly shaped nuclei, however, will certainly be larger than those obtained by this simple calculation, implying that the nuclear surface increased in the course of viral multiplication.

Nuclear surface. To examine the nuclear surface by cryo-FESEM, we used cells infected with BoHV-1 at an MOI of 10 and incubated for 7 and 12 h for rapid freezing under high pressure, subsequent freeze-etching, unidirectional shadowing with platinum, and immediate examination. Infected cells incubated for 7 h had nuclei with numerous nuclear pores containing pore complexes, similar to those found in uninfected cells, of about 120 nm in diameter (Fig. 2A and B). Some of the nuclear pores were enlarged up to 400 nm, as confirmed by LTEM (Fig. 2C to H). In a few cells, many dome-like structures measuring 140 to 190 nm protruded into the perinuclear space. Size and shape make these protrusions very likely to be capsids at different stages of budding, as shown below by LTEM. At 12 h of incubation, nuclei were found to contain not a single nuclear pore. Instead, there were budding capsids with indentations of 50 to 180 nm, some containing budding capsids, and bulges of up to 500 nm (Fig. 3A and B). The indentations most probably represent the result of the budding process immediately after completion (Fig. 4E). Bulges of various sizes, some of them broken away during fracturing, were found by LTEM to be due to dilation of nuclear pores through which nuclear material containing capsids had projected into the cytoplasm (Fig. 3C to F). The border between nuclear material and cytoplasm was always distinct, indicating that the two compartments did not merge. Apart from impaired nuclear pores, the nuclear surface was intact (Fig. 3C). Impaired nuclear pores were not found in uninfected cells. The number and degree of dilation, size of bulges, and number of capsids within the escaping nuclear material and cytoplasmic matrix increased drastically from 7 to 12 h of incubation.

Nuclear membranes. For investigation of the cell membranes involved in envelopment, cells infected at an MOI of 1, 5, or 10 were incubated from 3 to 40 h. Cells were arrested by high-pressure freezing, freeze substituted (LTEM), and embedded in such a way that sections could be cut parallel to the smooth surface obtained by removing the sapphire disk. To determine the nature of the gaps in the nuclear membranes, we chose sections cut perpendicularly to the nuclear surface. Nuclei of both infected and uninfected cells clearly revealed intact 100-nm-wide nuclear pores (Fig. 2C) with a distinct central layer corresponding to the central ring and a cloudy layer corresponding to the cytoplasmic ring and filaments of the nuclear pore complex (29). Gaps in the nuclear membrane measured 140 to 400 nm early in infection (defined as an MOI of 0.5 at 24 to 28 h, an MOI of 1 and 5 at 12 to 16 h, and an MOI of 10 at 3 to 5 h) (Fig. 2D to H) and up to 1,900 nm late in infection (defined as an MOI of 0.5 at 40 to 42 h, an MOI of 1 and 5 at 33 to 40 h, and an MOI of 10 at 12 to 14 h) (Fig. 3D to F). Dilations of 140 to 200 nm were already found in cells incubated for only 5 h at an MOI of 10. They were distinctly bordered by the inner nuclear membrane continuing into the outer nuclear membrane and thus were assumed to represent impaired nuclear pores lacking nuclear pore complex structures. Capsids were often present in front of (Fig. 2G and 3D), within (Fig. 3F), and close to (Fig. 2D and H and 3D) impaired nuclear pores.

LTEM also revealed capsids at various stages of budding through the inner nuclear membrane (Fig. 4A, C, and D). The capsid in intimate contact with the inner nuclear membrane (Fig. 4C) is considered to be in an initial phase of budding pushing the membrane slightly into the perinuclear space. In an intermediate phase (Fig. 4D), both the inner and outer nuclear membranes are pushed far into the cytoplasm. The inner nuclear membrane is thickened by a dense material that reaches exactly from one site where it turns into the perinuclear space to the other site. The membrane needs to be pulled at this turn behind the capsid for fusion to occur, which results in a fully enveloped virion and a deep indentation (Fig. 4E) also recognizable by cryo-FESEM (Fig. 3B). Fully enveloped virions were found in the perinuclear space (Fig. 4F), in conjunctions with associate cisternae (Fig. 4B) and within associated RER cisternae (Fig. 4G). They always exhibited a thick dense envelope that was nearly always in close contact to both the inner and outer nuclear membrane.

Although one might conclude from Fig. 2A that budding at the inner nuclear membrane is a frequently occurring event, we very rarely found budding by LTEM (Table 1). Indeed, we have only a few more micrographs convincingly demonstrating budding capsids at the inner nuclear membrane. Interestingly, we found more capsid-membrane interaction at the outer nuclear membrane than at the inner nuclear membrane. Because of the widely accepted theory that the envelope derived by budding through the inner nuclear membrane fuses with the outer nuclear membrane to release the capsid into the cytoplasm, we paid especial attention to this process. However, the trial designed to test our findings with the fusion theory failed. LTEM rather revealed budding events than fusion events. The capsids in close contact to the outer nuclear membrane, which is slightly pushed toward the perinuclear space (Fig. 5B to D) and slightly thickened (Fig. 5C and D), are considered more likely to be nearing the budding stage than the result of fusion, because the relation of capsids to the outer nuclear membranes exactly resembles that with the inner nuclear membrane (Fig. 4C and 5C). The intermediate states of the process taking place at the outer nuclear membrane (Fig. 5E to G) are characterized by the thickened membrane bending deep into the perinuclear space, exactly as such bending is caused by budding capsids at the inner nuclear membrane. The thickened membrane reaches from one side, where the outer nuclear membrane turns into the perinuclear space to the other side. The length of the thickened membrane equals about two-thirds of the final entire envelope, as does the thickening of inner nuclear membrane. The only difference from the inner nuclear membrane is that the inner membrane turns next to the nucleus are less than 90° or even zero (Fig. 5F), whereas it is 180° on the opposite side, so that the thickened envelope runs in parallel with the outer nuclear membrane for about 100 nm. To the best of our knowledge, this cannot happen in the course of fusion. We, hence, consider the data shown in Fig. 5E to 5G to represent intermediate phases of budding. Consequently, capsids (Fig. 5H and I) are assumed to be close to completion of budding into the perinuclear space at a narrow angle in relation to the outer nuclear membrane, which also makes the typical turn of 180°. Interestingly, the capsid shown in Fig. 5H

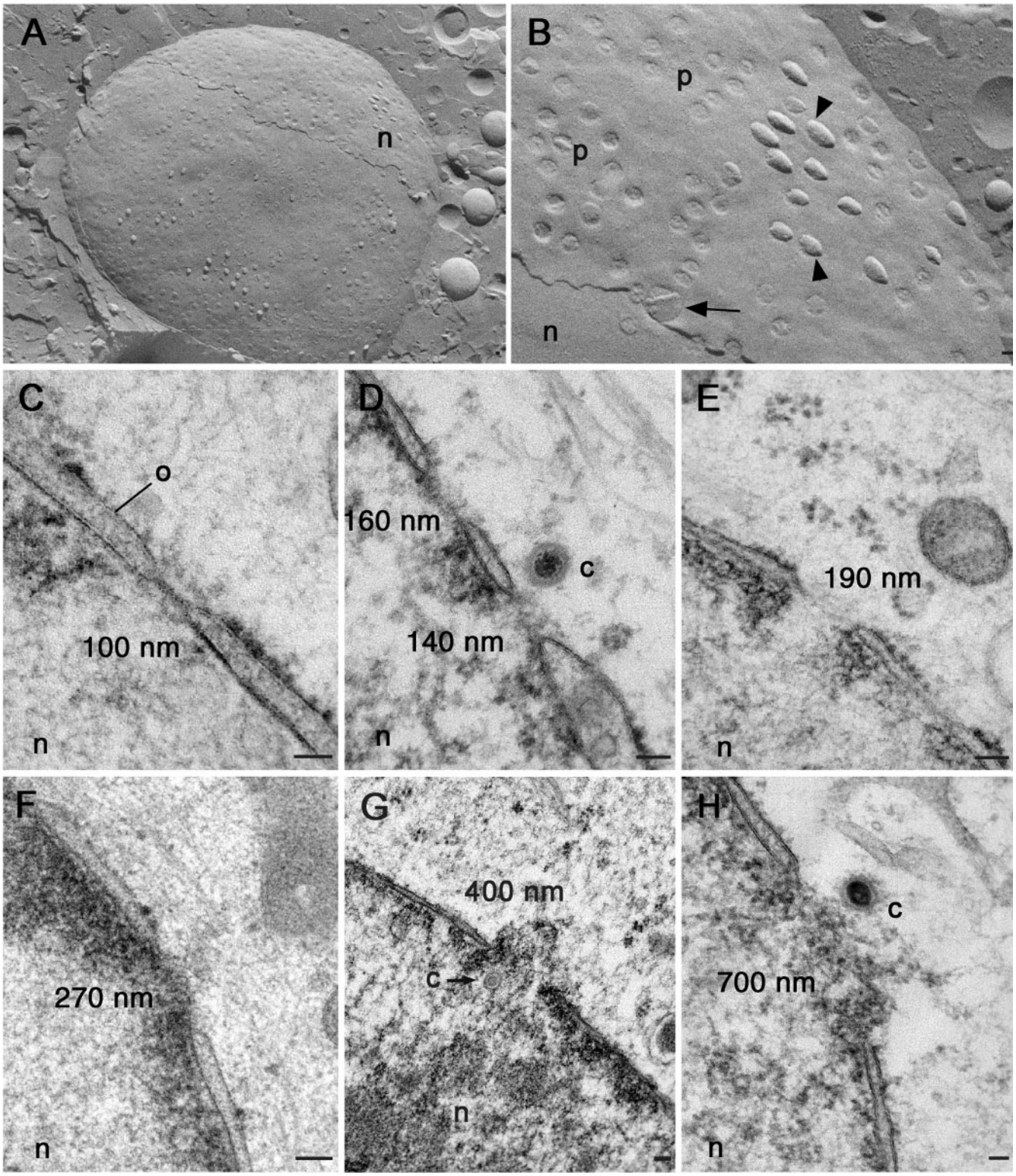

FIG. 2. Nuclear surface of MDBK cells early in infection with BoHV-1 at an MOI of 10 (A to D), 5 (E and H), or 1 (F and G). n, nucleus. (A and B) Cryo-FESEM images reveal intact nuclear pores (p), budding capsids (arrowheads) and a dilated nuclear pore (arrow). (C to H) TEM images of sections cut perpendicular to the nuclear surface. (C) Intact nuclear pore with distinct central density corresponding to the central plug of the nuclear pore complex and distinctly visible inner and outer (o) nuclear membrane. (D to H) The diameter of nuclear pores, defined by the border where the intact inner nuclear membrane merges with the outer nuclear membrane, is enlarged from 140 up to 700 nm. Nuclear content is within the border delineated by nuclear membranes in dilated pores up to about 200 nm (E), arches through impaired pores with diameters of about 300 nm (F), and bulges into the cytoplasm through more severely dilated pores (G and H). Capsids (c) are either just outside (D) but still in contact with (H) nuclear material or within nuclear material (G), suggesting that they are released via impaired nuclear pores. Bars, 1 μm (A); 100 nm (B to H).

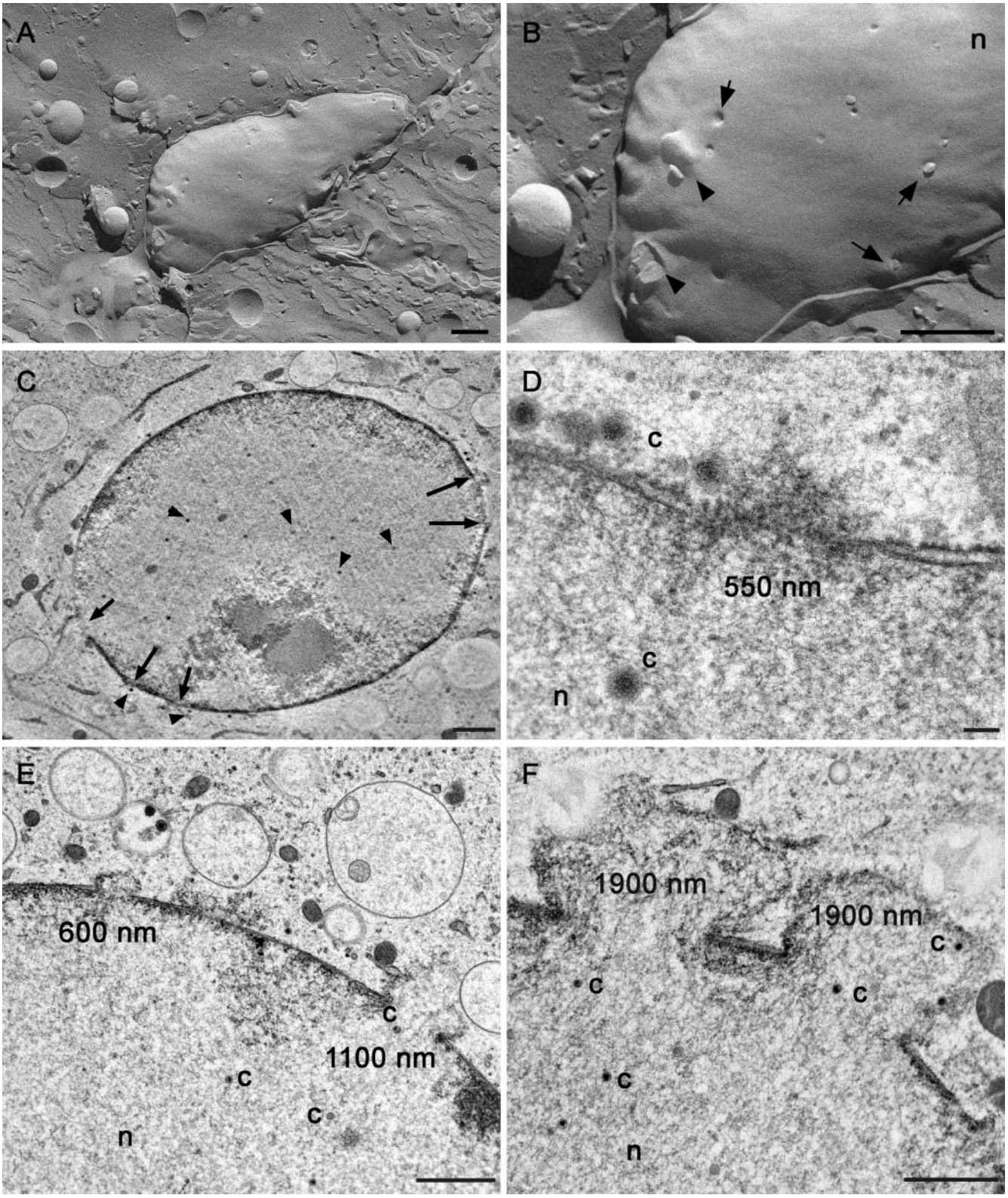

FIG. 3. The nuclear surface of MDBK cells late in infection with BoHV-1 at an MOI of 10 (A, B, and D), 5 (C and E), or 1 (F). (A and B) Cryo-FESEM images reveal a few budding capsids or holes, most probably indicating that budding has already been completed (arrows). Nuclear pores are not visible. Instead, there are protrusions of nuclear matrix (arrowheads); one broke away during freeze-etching. (C to F) LTEM images of intact nuclei with distinctly defined nuclear pores that are dilated up to 1,900 nm. Nuclear matrix containing capsids (c) protrudes into the cytoplasm but does not merge with it. Bars, 1 μm (A to C, E, and F); 100 nm (D).

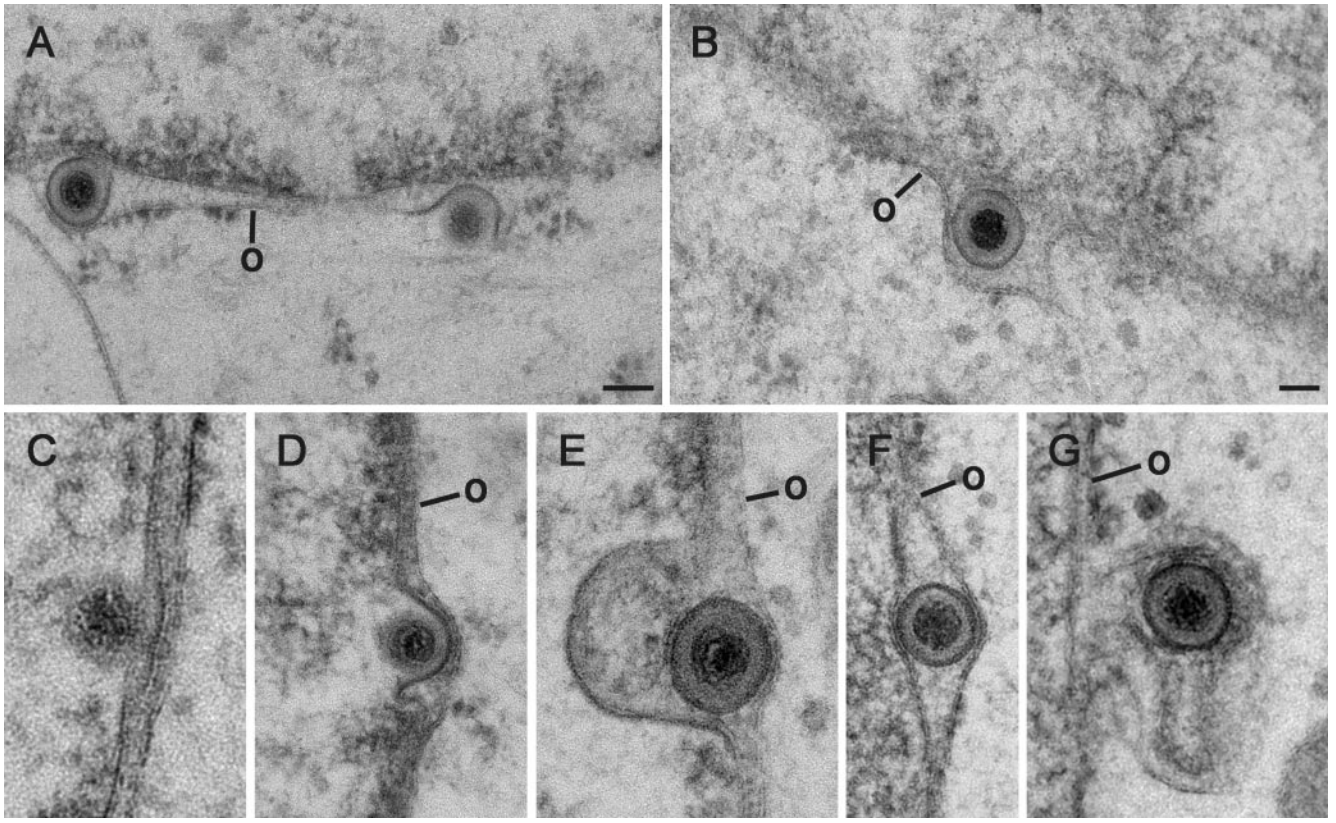

FIG. 4. The inner nuclear membrane and the perinuclear space early in infection at an MOI of 1 (A and B) or 10 (C to G). (A) At the left is a capsid close to completion of budding at the inner nuclear membrane containing a dense envelope that is in close apposition to the outer nuclear membrane (o). At the right is a capsid with about three-fourths of the entire envelope acting as part of the outer nuclear membrane. The tegument is only present between the capsid and the membrane, which is turned almost 180° at one side. This process is described in the legend to Fig. 5. (B) Virion with a dense envelope in the perinuclear space that continues into RER cisterna. (C) Initial phase of a budding capsid at the inner nuclear membrane. Slight thickening of the nuclear leaflet and the course of the membrane underneath the capsid are demonstrated because of underfocusing. (D) Intermediate phase of budding with distinct thickening of the inner nuclear membrane that is sharply bent at one side. Some tegument is deposited around the capsid. To form an enveloped particle, the membrane must be pulled into the nucleus behind the capsid for fusion. (E) Virion within the perinuclear space, probably shortly after budding was completed because of the large indentation of the inner nuclear membrane. (F) Virion within the perinuclear space with a dense layer at the envelope that is in close apposition to both the inner and the outer nuclear membrane. (G) Virion within a cisterna contiguous to the perinuclear space, implying an intracisternal transport. Bars, 100 nm.

buds at the site where the perinuclear space continues into an associated cisterna, the envelope is only four-fifths of its final length, and tegument is lacking at the site where the membrane needs to fuse for fission. In the results shown in Fig. 5I, tegumentation is completed, and the membrane is close to fusion or even in fusion, which results in fission of the enveloped virion from the outer nuclear membrane. There is no indication of fusion of the thickened envelope with the outer nuclear membrane; at this site, fusion would be expected if it occurred.

TABLE 1. Distribution of virus particles in 20 cellular profiles chosen at random in ultrathin sections of MDBK cells incubated for 16, 20, and 40 h with BoHV-1 at an MOI of 1[a]

h	Nca	Budding			Packaging		Wrapping			I-PN
		IM	OM	PS	Go	Vac1	Cca	Go	Vac2	
16	180	1	2	3	22	62	51	20	41	7
20	410		1	2	27	137	93	23	35	6
40	470	1		1	2	23	310	35	17	11

[a] Nca, nuclear capsids; IM, inner nuclear membrane; OM, outer nuclear membrane; PS, perinuclear space and associated RER; Go, Golgi membranes; Vac1, large vacuoles (Fig. 3B to E) (43); Cca, cytoplasmic capsids; Vac2, small vacuoles (Fig. 6E); I-PN, impaired nuclear pores. Note that numbers of viral particles and their distribution vary considerably among cells.

Golgi complex. Hundreds of capsids were found in the cytoplasm (Table 1), many of them approaching (Fig. 6A) or being enveloped by Golgi membranes. Capsids approached membranes at any site of the Golgi complex, most frequently, however, at the site closest to the nucleus (Fig. 6A, B, and D). Envelopment by Golgi membranes, termed wrapping, is analogous to budding at nuclear membranes. Budding starts by bending of the membrane at the site of close contact into Golgi cisterna and concomitant deposition of dense substance at the bending membrane (Fig. 6B). Subsequently, tegument is deposited between membrane and capsid, and bending proceeds, involving the entire membrane of the cisterna (Fig. 6C). To form an envelope, the membrane must be pulled behind the capsid and tegument for fusion that leads to an enveloped virion by fission from the Golgi membrane (Fig. 6D). Because the entire cisterna is involved, a vacuole is formed that needs to be detached (Fig. 6D). Spikes are distinctly visible in the

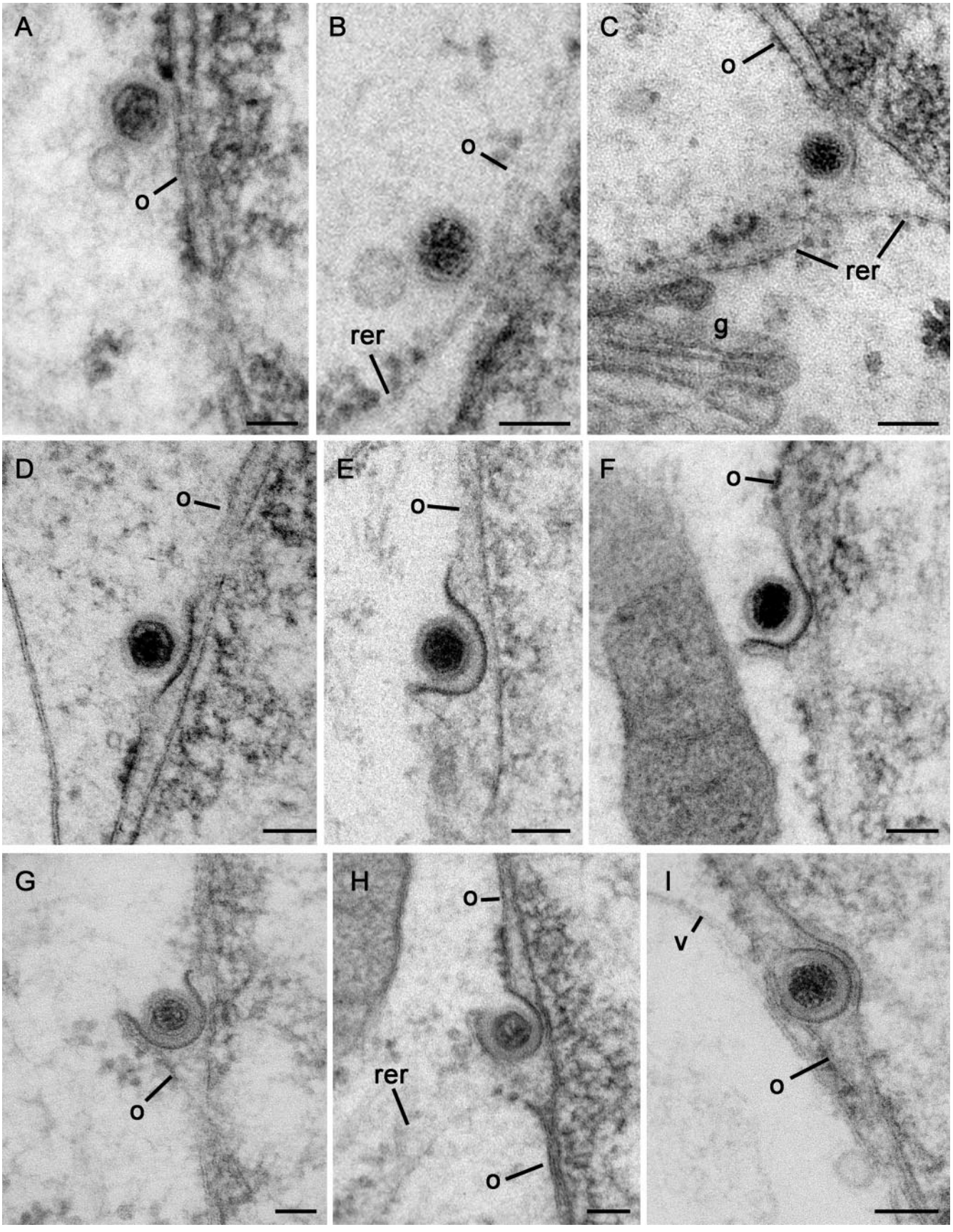
A
o
B
o
rer
C
o
rer
g
D
o
E
o
F
o
G
o
H
o
rer
o
I
v
o

process of envelopment. The vacuoles containing the fully enveloped virion are spheres with the virion in their center. The concentric space between envelope and vacuolar membrane is occupied by dense substance that seems to cover spikes (Fig. 6D to F). The vacuoles transport the virions toward the cell periphery, where the vacuolar membrane fuses with the plasma membrane (Fig. 6F), and the virion with its envelope full of spikes is released into the extracellular space (Fig. 6G). Apart from envelopment of approaching capsids from the cytoplasm, the Golgi complex is involved in packaging of virions, leading to entirely different vacuoles containing one or several virions with envelopes exhibiting distinct spikes (43). Golgi complexes dramatically increased after 5 h of incubation at an MOI of 10 and at 12 to 16 h at MOI of 1 and 5, compared to control cells. The Golgi complex, however, often consisted of only one or two cisternae or even of remnants in cells late in infection.

DISCUSSION

Infected MDBK cells produced and accumulated GFP-labeled capsids, virions, and proteins for many hours and suddenly disintegrated within a few minutes. Disk-like nuclei of cells at the beginning of incubation turned into disk-like nuclei with slightly decreased long diameters, increased short diameters of about 40%, and highly irregular surfaces. In an attempt to investigate the nuclear surface early in infection, we discovered distortions of nuclear pores involving the loss of nuclear pore complexes and enlargement of pore diameters from 140 up to 1,900 nm, while the nuclear membranes remained intact. The diameter of isolated nuclear pore complexes is 125 nm (29). We measured diameters of intact pores by LTEM as 100 to 110 nm. The discrepancy is probably due to section thickness that does not allow precise measurements. At the site of both intact and impaired nuclear pores, the inner nuclear membrane turns into the outer nuclear membrane. Impairment of nuclear pores was obvious also by CTEM (data not shown) and nicely documented in nuclei late in infection with simian agent 8 (2).

Impairment of nuclear pores raises the question as to whether or not it plays an essential role in rapid cell disintegration. To answer this is a difficult task and impossible on the basis of our data. The facts, however, that nuclear pore impairment had already occurred 7 h after infection in cells that were active in viral envelopment and had all other cellular structures intact and that cells accumulating virus remained active in terms of viral production for many hours and then disintegrated within a few minutes suggest that nuclear pore impairment per se is not responsible for cell death. The presence of capsids at sites of impaired nuclear pores suggests that capsids use these pores as gateways to the cytoplasm, as was supposed for simian agent 8 (2). This idea is supported by the low frequency of budding capsids encountered at the inner nuclear membrane and by the absence of any convincing fusion events at the outer nuclear membrane.

There may be two reasons for the low frequency of detectable budding capsids. Either the process is very rapid so that the chance to hit a capsid at the very moment of budding is low, or budding is a rare event. Fusion between influenza virus and liposomes is completed within 1 min (19). Budding at the inner nuclear membrane involves thickening of the nuclear membrane, driving the capsid toward the perinuclear space, deposition of tegument, and fusion of the inner nuclear membrane so that the enveloped virion can be detached. Considering that the fusion process alone takes 1 min, the entire budding process will take much longer. Hence, one must assume that budding ought to be seen easily if the frequency of budding were high. Indeed, budding can be visualized by cryo-FESEM impressively early in infection (Fig. 2). Budding can also be demonstrated very easily at Golgi membranes at almost any point in infection when envelopment has started. Budding at Golgi membranes is a process very similar to budding at the inner nuclear membrane. It involves deposition of dense substance at the membrane, driving the capsid toward Golgi cisternae, deposition of tegument, and fusion of Golgi membranes so that the envelope can be detached, finally lying in a vacuole that is derived by fission of Golgi membranes. In addition, the concentric space between envelope and vacuolar membrane is filled with a dense substance, a finding that had been demonstrated as early as 1988 (24). We assume that this dense substance has the same function as the substance deposited at the membrane during budding at nuclear membranes. Although wrapping by Golgi membranes is slightly more complicated than budding at the nuclear membrane, the time required for wrapping is probably not much longer than that of budding, because fission of the envelope may be overlapped by fission of the transport vacuole. It is thus fair to assume that the chance of hitting a budding capsid at the inner nuclear membrane is equal to that of hitting one at the Golgi membranes, provided the number of capsids is the same. Considering that the nucleus is hit in many more sections through a given cell than the Golgi complex, budding capsids at the inner

FIG. 5. The outer nuclear membrane and the perinuclear space early in infection, at an advanced stage of infection (defined as MOIs of 1 and 5 at 20 to 23 h, or an MOI of 10 at 7 to 8 h), and late in infection: an MOI of 5 (A to C), 1 (D, F, and H), or 10 (E, G, and I). (A) Capsid in intimate contact to the outer nuclear membrane (o) at a site free of ribosomes next to a dilated nuclear pore. (B) Capsid in intimate contact to the outer nuclear membrane that is slightly bent toward the perinuclear space. (C) Capsid in intimate contact to the outer nuclear membrane that is thickened and slightly bent toward the perinuclear space. The perinuclear space is continuous to the RER (rer) in contact with a Golgi membrane (g). (D) Capsid in intimate contact to the outer nuclear membrane distinctly thickened and bent. There is little or no tegument between the capsid and membrane. Panels A to D are considered to represent initial phases of budding at the outer nuclear membrane. (E to G) Capsids at the outer nuclear membrane that is markedly thickened and bent into the perinuclear space. The membrane turns close to 180° at one side of the capsid that is clearly separated from the membrane by tegument. These are considered to be intermediate phases of budding. (H) Capsid at the thickened outer nuclear membrane that bends deeply into the perinuclear space just at the site where it is contiguous with an RER cisterna. The outer nuclear membrane makes also a turn of close to 180° at one side of the capsid. The space between the membrane and the capsid is filled by tegument. (I) Capsid within the perinuclear space surrounded by tegument and the outer nuclear membrane that turns 180° at the cytoplasmic side. v, membrane of an empty vacuole. Bars,100 nm.

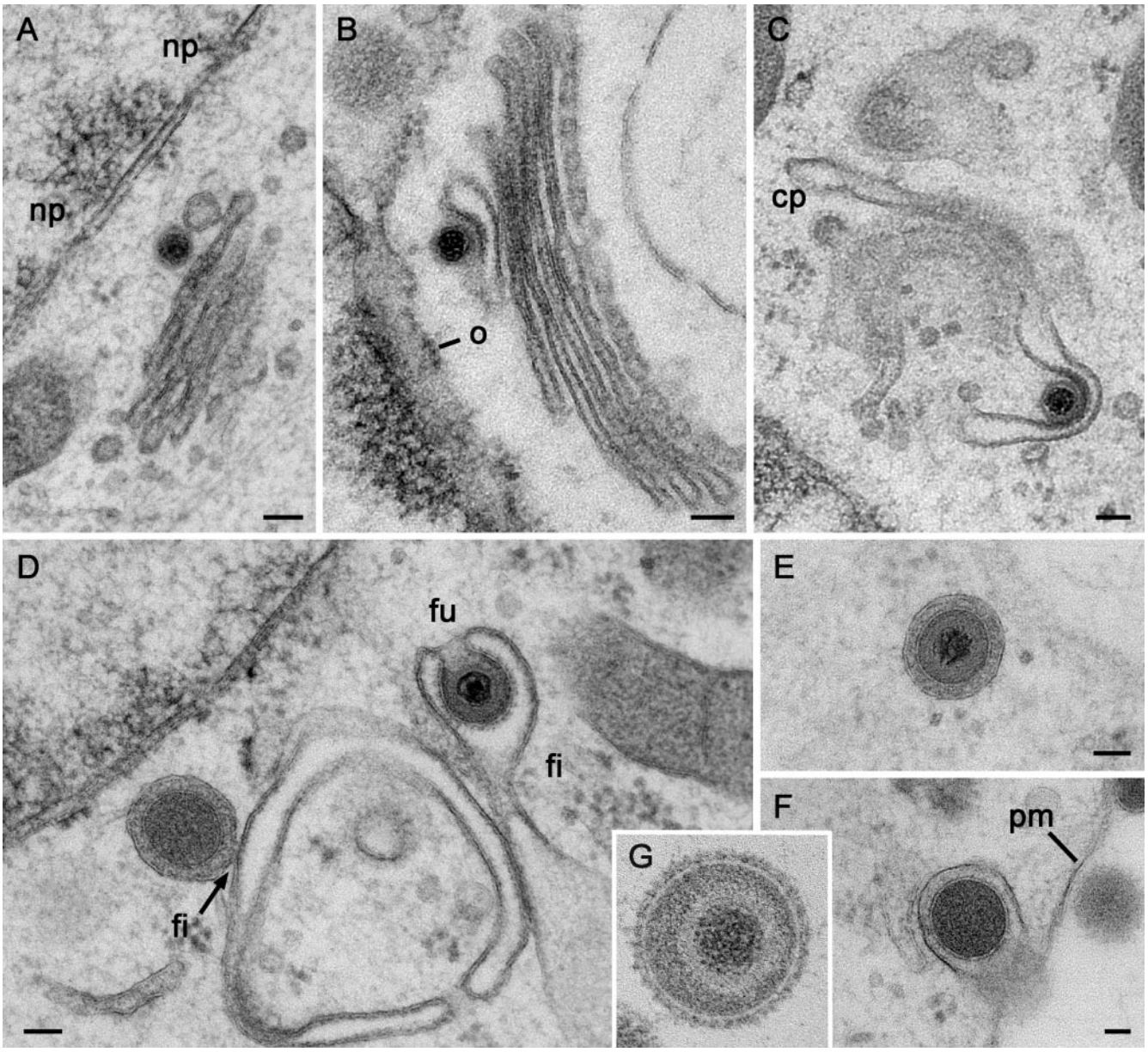

FIG. 6. Budding capsids at Golgi membranes and formation of transport vacuoles (wrapping) at advanced and late stages of infection, at an MOI of 1 (F), 5 (B, C, and E), or 10 (D and G). (A) Capsid approaching a Golgi membrane close to two dilated nuclear pores (np). (B) Capsid less than 100 nm from the outer nuclear membrane (o), in initial phase of budding with slight bending and thickening of the membrane in contact with the capsid. (C) Intermediate phase of budding with thickening of the membrane and little deposition of tegument. cp, coated pit. (D) Late phase of budding with tegument surrounding the capsid, clearly visible spikes, and start of fusion (fu) of Golgi membranes at the basal pole; wrapping is initiated by initation of fission (fi; right) but is close to completion at the left (fi; arrow) forming a spherical vacuole containing the virion (tangentially sectioned) and a dense substance completely hiding the spikes. (E) Spherical transport vacuole comprising a virion and dense substance-hiding spikes. (F) The membrane of a transport vacuole with a tangentially sectioned virion fuses with the plasma membrane (pm) releasing virion and antifusion proteins into the extracellular space. (G) Virion in the extra cellular space, comprising capsid with dense core, tegument, and envelope with spikes. Bars, 100 nm.

nuclear membrane ought to be encountered very frequently. Since this is certainly not the case, it is reasonable to assume that budding at the inner nuclear membrane is a rare event.

If the fusion theory were correct, the number of budding capsids at the inner nuclear membrane would equal the number of envelope fusions with the outer nuclear membrane. Fusion certainly would be faster than budding, meaning that the chance of hitting an envelope in fusion is less than that of hitting a budding capsid. Interestingly, our results demonstrate that the number of capsids involved in the process at the outer nuclear membrane is higher than that at the inner nuclear membrane. To draw a final conclusion from this low number of events encountered with hundreds of cells is not possible. Together with the following consideration, however, this obser-

vation definitely does not support the fusion theory. The surface area of a virion with a diameter of 200 nm (17, 45) is 0.125 μm^2. The surface of 1,000 virions—a number reasonably assumed to be produced by one cell—equals the surface area of a sphere-like nucleus with a diameter of 6.3 μm or approximately of a disk-like nucleus with axes of 18.5, 16, and 2.5 μm, giving a surface of 133 μm^2 (Fig. 1). This means that the entire inner nuclear membrane would be inserted into the outer nuclear membrane, which in turn would need to be shifted to the inner nuclear membrane at the site they meet each other (the nuclear pores) within a few hours. We do not know whether or not this shift is possible. However, it seems rather difficult because of the steady interference by the budding and the fusion processes. Furthermore, cell volume and cell surface area increased, although only slightly, in the course of virus production, implying either additional membrane supplementation or augmentation of the surface area exclusively due to enlargement of nuclear pores. Another crucial point is the thickening of the membrane that becomes the viral envelope, as shown by many other authors (1, 2, 7, 9, 12, 16, 22, 30, 33). What is the role of the membrane thickening? Why would it disappear immediately after fusion with the outer nuclear membrane? And why is it present in virions within the perinuclear space and even in its associated cisternae? There is no answer to this from the standpoint of the fusion theory.

A plausible significance of this membrane, thickened due to the deposition of a dense substance, a protein(s) of as-yet-unknown nature, is to prevent the envelope from fusion with the outer nuclear membrane, the inner nuclear membrane, and the membranes of those cisternae through which the virion is transported. If virions can be transported within the perinuclear space into associated cisternae, and there are many indications that they do (2, 4, 6, 8, 9, 11, 12, 16, 31, 33, 34, 42)–, the viral envelope must be unable to fuse. Alternatively, if the viral envelope could fuse with the outer nuclear membrane, it could probably also fuse with the inner nuclear membrane; certainly, it cannot be transported within spaces where those membranes need to be in close contact with the envelope simply, because of size differences. The theoretical considerations are well supported by the morphology of the process taking place at the outer nuclear membrane. (i) Capsids in close contact with the membrane, which may be slightly bent into the perinuclear space, are very difficult to imagine once released from the perinuclear space by fusion. (ii) Membranes in fusion do not make 180° turns (Fig. 5). Fusion of membranes starts by close apposition, followed by formation of fusion stalks and finally of fusion pores (21, 25, 26), a process of high symmetry that can be visualized by electron microscopy employing cryotechniques (19). (iii) The envelope-membrane interaction at the outer nuclear membrane shows high identity with the process of budding capsids at the inner nuclear membrane. The only difference between the processes at the inner and the outer nuclear membrane is the angle between the axis of capsid movement and the nuclear periphery. This angle is about 90° at the inner membrane and 30 to 40° at the outer nuclear membrane. Budding capsids at the inner nuclear membrane are driven toward the outer nuclear membrane that can give way by projecting into the cytoplasm. Capsids budding at the outer nuclear membrane must be driven at a narrow angle into the perinuclear space because the nucleus is solid compared to the cytoplasmic matrix. Indications for budding at the outer nuclear membrane were also published for herpes simplex virus 1 (23) and simian agent 8 (2).

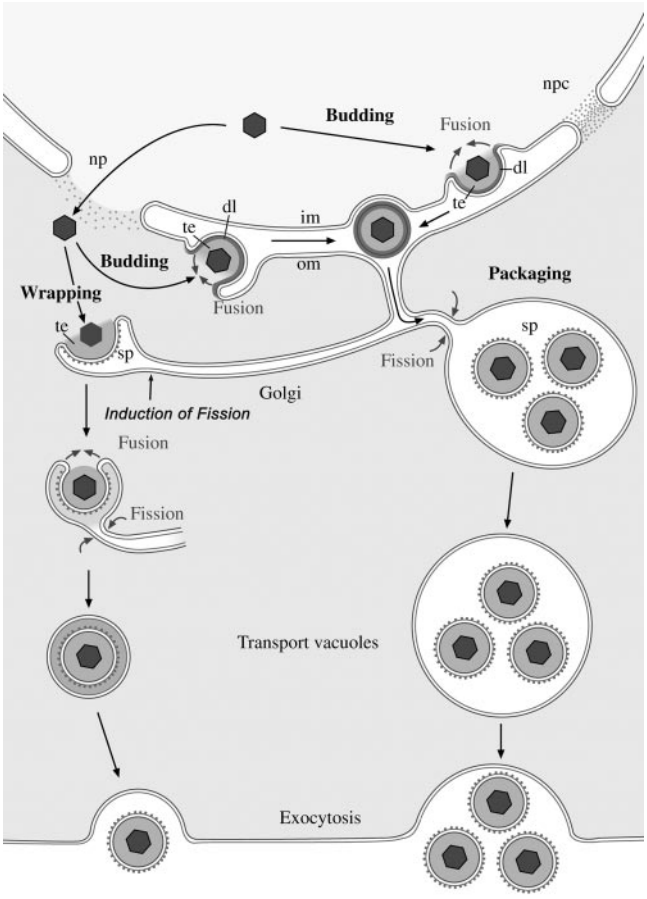

FIG. 7. Schematic drawing of the dual pathway of BoHV-1 envelopment. In the wrapping pathway, capsids leave the nucleus via impaired nuclear pores (np) and approach Golgi membranes from the cytoplasmic side, inducing budding. Since the entire cistern is involved, a sphere-like structure comprising two membranes arises. The inner membrane becomes the viral envelope, and the outer becomes the vacuolar membrane. Fusion of the envelope with the vacuolar membrane is prevented by antifusion proteins at high concentrations. In the packaging pathway, capsids bud through the inner or outer nuclear membrane and are transported from the perinuclear space via RER cisternae into Golgi cisternae for packaging into transport vacuoles of various sizes containing one or more virions. The fusion of viral envelope with cell membranes is prevented by proteins of as-yet-unknown nature localized at the viral envelope. The antifusion proteins are cleft off in Golgi cisternae but remain there (possibly together with additional proteins at low concentration) to prevent fusion of viral envelopes with the membrane of large transport vacuoles. im, inner nuclear membrane; om, outer nuclear membrane; npc, nuclear pore complex; dl, dense layer (antifusion proetein); sp, spikes; te, tegument.

If capsids are not released into the cytoplasm by fusion, what is the fate of the virions derived by budding at the nuclear membranes? As mentioned above, they are transported into associated RER cisternae. RER cisternae have been shown to continue into Golgi cisternae (28, 40, 43). Consequently, virions can be transported directly from the perinuclear space via RER cisternae into Golgi cisternae (43). There, they are pack-

aged into transport vacuoles that are entirely different from transport vacuoles derived from wrapping. Vacuoles originating from packaging are of various sizes containing one or more virions with an envelope missing the dense layer. Instead, spikes are clearly apparent; the space between the viral envelopes and vacuolar membrane is not occupied by the dense material, as in concentric vacuoles derived by wrapping. This substance is assumed to prevent the viral envelope from fusion with the vacuolar membrane. It thus is speculated that it is the same substance that is deposited at the viral envelope in the course of budding at nuclear membranes. The same substance might be present also in large vacuoles derived by packaging though at lower concentrations.

Taken together, the two sorts of transport vacuoles imply diverse pathways of capsids through the Golgi complex (Fig. 7). One pathway involves budding at Golgi membranes, resulting in a centrally located virion within a small vacuole containing antifusion protein at high concentrations. This pathway is designated the wrapping pathway. In the other pathway, virions, whose envelope and tegument originated by budding at nuclear membranes, are covered by an antifusion protein and hence can be transported within the perinuclear space and associated RER cisternae into Golgi cisternae for packaging into large vacuoles. The antifusion protein covering the viral surface is cleft off, possibly remaining together with additional antifusion proteins within vacuoles. This pathway is designated the packaging pathway. Packaging and wrapping may take place simultaneously at the same Golgi complex (43). The number of capsids that bud at the inner nuclear membrane is probably low and higher early in infection. Capsids approaching Golgi membranes from the cytoplasmic side escape from the nucleus via impaired nuclear pores. Capsids have the ability to induce budding at the nuclear side and the cytoplasmic side of cell membranes, provided the machinery necessary for the budding process is present.

ACKNOWLEDGMENTS

We thank Bernard Roizman for critical discussion of data, Jeanne Peter for drawing Fig. 7, and the referees for helpful comments.

The study was supported by Stiftung für Wissenschaftliche Forschung an der Universität Zürich.

REFERENCES

1. **Baines, J. D., R. J. Jacob, L. Simmerman, and B. Roizman.** 1995. The herpes simplex virus 1 UL11 proteins are associated with cytoplasmic and nuclear membranes and with nuclear bodies of infected cells. J. Virol. **69:**825–833.
2. **Borchers, K., and M. Oezel.** 1993. Simian agent 8 (SA8): morphogenesis and ultrastructure. Zentralbl. Bakteriol. **279:**526–536.
3. **Brown, S. M., A. R. MacLean, J. D. Aitken, and J. Harland.** 1994. ICP34.5 influences herpes simplex virus type 1 maturation and egress from infected cells in vitro. J. Gen. Virol. **75:**3679–3686.
4. **Browne, H., S. Bell, T. Minson, and D. W. Wilson.** 1996. An endoplasmic reticulum-retained herpes simplex virus glycoprotein H is absent from secreted virions: evidence for reenvelopment during egress. J. Virol. **70:**4311–4316.
5. **Campadelli-Fiume, G., F. Farabegoli, S. Di Gaeta, and B. Roizman.** 1991. Origin of unenveloped capsids in the cytoplasm of cells infected with herpes simplex virus 1. J. Virol. **65:**1589–1595.
6. **Card, J. P., L. Rinaman, R. B. Lynn, B. H. Lee, R. P. Meade, R. R. Miselis, and L. W. Enquist.** 1993. Pseudorabies virus infection of the rat central nervous system: ultrastructural characterization of viral replication, transport, and pathogenesis. J. Neurosci. **13:**2515–2539.
7. **Church, G. A., and D. W. Wilson.** 1997. Study of herpes simplex virus maturation during a synchronous wave of assembly. J. Virol. **71:**3603–3612.
8. **Di Lazzaro, C., G. Campadelli-Fiume, and M. R. Torrisi.** 1995. Intermediate forms of glycoconjugates are present in the envelope of herpes simplex virions during their transport along the exocytic pathway. Virology **214:**619–623.
9. **Fong, C. K., R. B. Tenser, G. D. Hsiung, and P. A. Gross.** 1973. Ultrastructural studies of the envelopment and release of guinea pig herpes-like virus in cultured cells. Virology **52:**468–477.
10. **Fraefel, C., M. Ackermann, and M. Schwyzer.** 1994. Identification of the bovine herpesvirus 1 circ protein, a myristylated and virion-associated polypeptide which is not essential for virus replication in cell culture. J. Virol. **68:**8082–8088.
11. **Gershon, A., L. Cosio, and P. A. Brunell.** 1973. Observations on the growth of varicella-zoster virus in human diploid cells. J. Gen. Virol. **18:**21–31.
12. **Gershon, A. A., D. L. Sherman, Z. Zhu, C. A. Gabel, R. T. Ambron, and M. D. Gershon.** 1994. Intracellular transport of newly synthesized varicella-zoster virus: final envelopment in the trans-Golgi network. J. Virol. **68:**6372–6390.
13. **Gilbert, R., K. Ghosh, L. Rasile, and H. P. Ghosh.** 1994. Membrane anchoring domain of herpes simplex virus glycoprotein gB is sufficient for nuclear envelope localization. J. Virol. **68:**2272–2285.
14. **Gong, M., and E. Kieff.** 1990. Intracellular trafficking of two major Epstein-Barr virus glycoproteins, gp350/220 and gp110. J. Virol. **64:**1507–1516.
15. **Granzow, H.** 2001. Egress of alphaherpesviruses: comparative ultrastructural study. J. Virol. **75:**3675–3684.
16. **Granzow, H., F. Weiland, A. Jons, B. G. Klupp, A. Karger, and T. C. Mettenleiter.** 1997. Ultrastructural analysis of the replication cycle of pseudorabies virus in cell culture: a reassessment. J. Virol. **71:**2072–2082.
17. **Grunewald, K., P. Desai, D. C. Winkler, J. B. Heymann, D. M. Belnap, W. Baumeister, and A. C. Steven.** 2003. Three-dimensional structure of herpes simplex virus from cryo-electron tomography. Science **302:**1396–1398.
18. **Homman-Loudiyi, M., K. Hultenby, W. Britt, and C. Soderberg-Naucler.** 2003. Envelopment of human cytomegalovirus occurs by budding into Golgi-derived vacuole compartments positive for gB, Rab 3, trans-Golgi network 46, and mannosidase II. J. Virol. **77:**3191–3203. (Erratum, **77:**8179.)
19. **Kanaseki, T., K. Kawasaki, M. Murata, Y. Ikeuchi, and S. Ohnishi.** 1997. Structural features of membrane fusion between influenza virus and liposome as revealed by quick-freezing electron microscopy. J. Cell Biol. **137:**1041–1056.
20. **Klupp, B. G., J. Baumeister, P. Dietz, H. Granzow, and T. C. Mettenleiter.** 1998. Pseudorabies virus glycoprotein gK is a virion structural component involved in virus release but is not required for entry. J. Virol. **72:**1949–1958.
21. **Kozlovsky, Y., L. V. Chernomordik, and M. M. Kozlov.** 2002. Lipid intermediates in membrane fusion: formation, structure, and decay of hemifusion diaphragm. Biophys. J. **83:**2634–2651.
22. **Lecatsas, G., and G. Poste.** 1973. Mechanism of envelopment of herpesvirus by the nucelar envelope. Onderstepoort J. Vet. Res. **40:**71–72.
23. **Lopez-Iglesias, C., and F. Puvion-Dutilleul.** 1988. Visualization of glycoproteins after tunicamycin and monensin treatment of herpes simplex virus infected cells. J. Ultrastruct. Mol. Struct. Res. **101:**75–91.
24. **Lycke, E., B. Hamark, M. Johansson, A. Krotochwil, J. Lycke, and B. Svennerholm.** 1988. Herpes simplex virus infection of the human sensory neuron. An electron microscopy study. Arch. Virol. **101:**87–104.
25. **May, S.** 2002. Structure and energy of fusion stalks: the role of membrane edges. Biophys. J. **83:**2969–2980.
26. **Melikyan, G. B., and L. V. Chernomordik.** 1997. Membrane rearrangements in fusion mediated by viral proteins. Trends Microbiol. **5:**349–355.
27. **Metzler, A. E., A. A. Schudel, and M. Engels.** 1986. Bovine herpesvirus 1: molecular and antigenic characteristics of variant viruses isolated from calves with neurological disease. Arch. Virol. **87:**205–217.
28. **O'Donnell, C. M., K. Kaczman-Daniel, P. F. Goetinck, and B. M. Vertel.** 1988. Nanomelic chondrocytes synthesize a glycoprotein related to chondroitin sulfate proteoglycan core protein. J. Biol. Chem. **263:**17749–17754.
29. **Pante, N., and U. Aebi.** 1996. Molecular dissection of the nuclear pore complex. Crit. Rev. Biochem. Mol. Biol. **31:**153–199.
30. **Pol, J. M., F. Wagenaar, and A. Gielkens.** 1991. Morphogenesis of three pseudorabies virus strains in porcine nasal mucosa. Intervirology **32:**327–337.
31. **Radsak, K., M. Eickmann, T. Mockenhaupt, E. Bogner, H. Kern, A. Eis-Hubinger, and M. Reschke.** 1996. Retrieval of human cytomegalovirus glycoprotein B from the infected cell surface for virus envelopment. Arch. Virol. **141:**557–572.
32. **Rixon, F. J.** 1993. Structure and assembly of herpesviruses. Semin. Virol. **4:**135–144.
33. **Roller, R. J., Y. Zhou, R. Schnetzer, J. Ferguson, and D. DeSalvo.** 2000. Herpes simplex virus type 1 U_L34 gene product is required for viral envelopment. J. Virol. **74:**117–129.
34. **Schwartz, J., and B. Roizman.** 1969. Concerning the egress of herpes simplex virus from infected cells: electron and light microscope observations. Virology **38:**42–49.
35. **Studer, D., M. Michel, and M. Muller.** 1989. High pressure freezing comes of age. Scanning Microsc. Suppl. **3:**253–268.
36. **Tobler, K., C. Fraefel, and M. Ackermann.** 2002. Cloning of BoHV-1genome as a BAC and amplication-mediated creation of mutagenized BoHV-1, abstr. 5.26. 27th International Herpesvirus Workshop, Cairns, Australia.
37. **Torrisi, M. R., C. Di Lazzaro, A. Pavan, L. Pereira, and G. Campadelli-Fiume.** 1992. Herpes simplex virus envelopment and maturation studied by fracture label. J. Virol. **66:**554–561.

38. **Walther, P., and M. Müller.** 1997. Double-layer coating for field-emission cryo-scanning electron microscopy—present state and applications. Scanning **19:**343–348.
39. **Walther, P., E. Wehrli, R. Hermann, and M. Müller.** 1995. Double-layer coating for high-resolution low-temperature scanning electron microscopy. J. Microsc. **179:**229–237.
40. **Wang, Z. H., M. D. Gershon, O. Lungu, Z. L. Zhu, S. Mallory, A. M. Arvin, and A. A. Gershon.** 2001. Essential role played by the C-terminal domain of glycoprotein I in envelopment of varicella-zoster virus in the trans-Golgi network: interactions of glycoproteins with tegument. J. Virol. **75:**323–340.
41. **Weibull, C., and A. Christiansson.** 1986. Extraction of proteins and membrane lipids during low temperature embedding of biological material for electron microscopy. J. Microsc. **142:**79–86.
42. **Whealy, M. E., J. P. Card, R. P. Meade, A. K. Robbins, and L. W. Enquist.** 1991. Effect of brefeldin A on alphaherpesvirus membrane protein glycosylation and virus egress. J. Virol. **65:**1066–1081.
43. **Wild, P., E. M. Schraner, D. Cantieni, E. Loepfe, P. Walther, M. Muller, and M. Engels.** 2002. The significance of the Golgi complex in envelopment of bovine herpesvirus 1 (BHV-1) as revealed by cryobased electron microscopy. Micron **33:**327–337.
44. **Wild, P., E. M. Schraner, H. Adler, and B. M. Humbel.** 2001. Enhanced resolution of membranes in cultured cells by cryoimmobilization and freeze-substitution. Microsc. Res. Tech. **53:**313–321.
45. **Zhou, Z. H., D. H. Chen, J. Jakana, F. J. Rixon, and W. Chiu.** 1999. Visualization of tegument-capsid interactions and DNA in intact herpes simplex virus type 1 virions. J. Virol. **73:**3210–3218.
46. **Zhu, Z., M. D. Gershon, Y. Hao, R. T. Ambron, C. A. Gabel, and A. A. Gershon.** 1995. Envelopment of varicella-zoster virus: targeting of viral glycoproteins to the trans-Golgi network. J. Virol. **69:**7951–7959.